

Photon splitting corrections to soft-photon resummation

Lois Flower, Marek Schönherr

Institute for Particle Physics Phenomenology, Department of Physics, Durham University, Durham, DH1 3LE, UK

Abstract: In this paper we present an algorithm to add photon-splitting corrections to the Yennie-Frautschi-Suura-style soft-photon resummation available in the SHERPA Monte-Carlo event generator. Photon-splitting corrections enter at NNLO in QED and, as these effects are not incorporated in the standard QED FSR resummations, their size is larger than the pure hard photon-emission corrections at the same order. We introduce different lepton dressing strategies which incorporate further leptons and hadrons in addition to the customary photons, and discuss their sensitivity to dressing parameters such as the cone size. Finally, we quantify the effects of photon splittings into charged fermions and scalars under different such dressing strategies on $Z \rightarrow e^+e^-$ decays and find effects of up to 1% for suitably inclusive dressing strategies independent of the dressing cone size, and up to 9% if only photons are used in the dressing procedure with large dressing cones.

Contents

1	Introduction	2
2	Soft-photon resummation and photon splittings	3
2.1	The YFS soft-photon resummation	3
2.2	Photon splittings	4
2.3	Properties of the photon-splitting algorithm	8
3	Lepton dressing beyond photons	11
3.1	Dressing strategies in the presence of photon splittings	11
3.2	Case study: Z boson decay	14
4	Conclusions	15
A	Charged resonances	18
B	Usage	19

1 Introduction

Precision measurements of the Standard Model continue to stress-test our understanding of particle physics at an unprecedented level. In particular, charged and neutral Drell-Yan production at hadron colliders like the LHC are used as standard candles due to their large cross sections and exceedingly small experimental uncertainties, often below the percent level. However, these electroweak precision observables have also been brought to the forefront of searches for new physics, in the form of measured deviations from the Standard Model prediction. For example, the recent extraction of the W boson mass, performed by the CDF experiment on legacy Tevatron data [1], is in apparent tension with the world average [2] and previous hadron and lepton collider measurements [3, 4, 5, 6, 7, 8, 9, 10, 11, 12, 13, 14, 15, 16, 17, 18, 19, 20], as well as measurements of other fundamental EW parameters in Z production [21, 22, 23, 24, 25, 26, 27, 28, 29, 30]. Measurements such as this motivate precise theoretical input with uncertainties in the permille range or lower. At this level of required accuracy, higher-order QCD and electroweak corrections in vector-boson production must be supplemented with additional sources of theoretical precision. In addition to a consideration of the structure functions describing the make-up of the incident particles, a detailed description of the vector boson’s decay is paramount. Special emphasis must lie on the precise phase space distribution and flavour composition of the accompanying radiation, in order to be able to precisely model the detector response. With this paper we contribute to the effort to determine the size and uncertainty of higher-order QED corrections in the description of the decay of massive vector bosons.

Higher-order corrections to Drell-Yan processes are known to first order in the complete electroweak Standard Model [31, 32, 33, 34, 35, 36, 37, 38, 39, 40]. The recent advances at NNLO QCD-EW mixed calculations [41, 42, 43, 44, 45, 46, 47, 48, 49, 50], though an impressive achievement in their own right, have not increased the perturbative accuracy of the description of EW or QED radiative corrections themselves. Alternatively, universal QED corrections can be resummed to all orders either in traditional QED parton showers [51] by means of the DGLAP equation, or through the soft-photon resummation devised by Yennie, Frautschi, and Suura (YFS) [52]. These resummations can of course be matched to the fixed-order calculations mentioned above. A QED parton shower is available in all major Monte-Carlo event generators, HERWIG [53, 54], PYTHIA [55, 56], and SHERPA [57, 58, 59], while the YFS approach is implemented in HERWIG [60] and SHERPA [61, 62] for particle decays. The implementation in SHERPA has recently been extended to also resum initial-state soft-photon radiation in e^+e^- collisions [63].

To reach the necessary precision to make full use of the existing and future experimental datasets, the QED effects impacting the leptonic final state of the Drell-Yan process have to be understood in detail. These effects are driven by soft and collinear photon radiation. They can be resummed to all orders, and be further improved order by order in perturbation theory. Such calculations, matching to at least NLO EW corrections and sometimes even including NNLO QED ones, have been implemented using QED parton

showers in HORACE [64, 65, 66, 67, 68, 69] and POWHEG [70, 71, 72, 73], using the structure function approach in RADY [37, 38], and through a YFS-type soft-photon resummation in WINHAC/ZINHAC [74], HERWIG [60] and SHERPA [61, 62]. In addition, the PHOTOS Monte-Carlo [75, 76, 77, 78] provides an algorithm based on both soft-photon resummation and matrix element corrections. Dedicated comparisons between SHERPA’s YFS-type resummation and PHOTOS [79], between HORACE and PHOTOS [80], as well as HORACE and WINHAC [81] have yielded very good agreement.

A key element in the description of final state radiative corrections, however, has only been sporadically and not very systematically addressed: the possible splitting of the radiated bremsstrahlung photons into secondary charged-particle pairs. These corrections only enter at a relative $\mathcal{O}(\alpha^2)$ in Drell-Yan processes, but the production of light flavours may be enhanced logarithmically and thus gain relevance. In addition, and in contrast to QCD, photons and light charged flavours like electrons, muons, or pions, are experimentally distinguishable – such conversions alter the visible make-up of the final state and are thus of importance at the envisaged theoretical precision. It is also important to consider here the usual experimental and phenomenological practice of dressing charged leptons with photon radiation. While definitions of QCD jets have been constantly refined, there has been little discussion of dressed lepton algorithms since the adoption of cone-dressing strategies where all photons within a certain radius of the lepton are absorbed. Considering higher-order corrections in the form of photons splitting into charged particles has the potential to spoil the physically meaningful definition of a lepton dressed with photons. The treatment of charged leptons in the presence of secondary charged flavours must therefore be handled with care. Thus, while a first implementation of pair-production corrections exists in PHOTOS [82, 83], it only covers photon splittings into electrons and muons, and their theoretical and phenomenological impact has not been rigorously appraised. This paper addresses this issue by introducing a rigorous independent framework to calculate these corrections and study the resulting theoretical and phenomenological implications.

This paper proceeds as follows: We begin by providing a brief summary of the YFS soft-photon resummation as implemented in SHERPA before providing a comprehensive description of the photon splitting implementation, including a detailed examination of their interplay and the splitting properties in Sec. 2. We then present a detailed discussion of possible extensions of the standard lepton dressing algorithm to cope with the presence of secondary pairs of (light) charged particles, and quantify their effect on $Z \rightarrow e^+e^-$ decays in Sec. 3. Finally, we offer some concluding remarks in Sec. 4.

2 Soft-photon resummation and photon splittings

Incorporating photon-splitting processes alongside photon emissions are straightforwardly implemented when both are described in a common parton shower framework. We prefer, however, to base our implementation on the existing and superior description of photon emission corrections in the YFS framework of [61], including its inherent coherent-radiation formulation and existing NNLO QED and NLO EW corrections [62]. In this section we thus start by providing a brief summary of the Yennie-Frautschi-Suura (YFS) soft-photon resummation and its implementation in the SHERPA event generator. The remainder of this section then discusses the construction of photon splitting algorithm in detail before examining its properties.

2.1 The YFS soft-photon resummation

The work of Yennie–Frautschi–Suura (YFS) [52] describes the infrared singularities of QED to all orders. To achieve this, YFS consider all charged particles of the theory to be massive, and as a consequence only singularities associated with soft-photon emission are present. In particular, all photon splittings are finite and thus do not partake in the analysis of the infrared singular structure. Using that knowledge, the YFS algorithm reorders the perturbative expansion of a scattering or decay matrix element. This amounts to a resummation of the respective soft-photon logarithms in the enhanced real and virtual regions, leaving a perturbative expansion in infrared-finite, hard photons (both real emissions and virtual exchanges).

In the implementation of the YFS resummation in SHERPA for particle decays [61], the all-orders soft-photon resummed differential decay rate is written as

$$d\Gamma^{\text{YFS}} = d\Gamma_0 \cdot e^{\alpha Y(\omega_{\text{cut}})} \cdot \sum_{n_\gamma=0}^{\infty} \frac{1}{n_\gamma!} \left[\prod_{i=1}^{n_\gamma} d\Phi_{k_i} \cdot \alpha \tilde{S}(k_i) \Theta(k_i^0 - \omega_{\text{cut}}) \cdot \mathcal{C} \right], \quad (2.1)$$

wherein $d\Gamma_0$ is the leading-order (LO) differential decay rate and the YFS form factor $Y(\omega_{\text{cut}})$ contains the soft-photon logarithms. The decay rate is then summed over all possible additional photon emissions with an energy larger than ω_{cut} wrt. the leading-order decay. Each emission is described through its eikonal \tilde{S} and corrected for hard emission effects up to a given order through the correction factor \mathcal{C} .¹

Unlike a conventional parton shower, where the resummation is reliant on the factorisation of subsequent emissions when ordered in an evolution variable, YFS photons are unordered. In addition, they are also emitted coherently from the charged multipole through the radiator function \tilde{S} and are thus not inherently associated with a specific emitter particle. Consequently, when the produced final state is to be further treated by a dedicated photon-splitting parton shower, the existing configuration must be interpreted in the parton shower’s evolution and splitting language before any further splittings take place. Of course, care has to be taken so as to not compromise its leading logarithmic soft-photon resummation. In the following algorithm, since the effects added are completely beyond the scope of the YFS formulation without any potential overlap, this requirement amounts to ensuring the kinematic recoil induced by a splitting photon on the primary charged particle ensemble (and possibly other existing photons), vanishes in the limit that the energy of the splitting photon vanishes. While this is trivially true as all charged particles are treated as massive, the recoil assignment performed in this study and described in section 2.2 introduces corrections to the momenta of the primary charged particle ensemble which scale non-logarithmically with the photon energy and hence do not contribute to the leading-logarithmic resummation.

2.2 Photon splittings

In this section we introduce the parton shower algorithm which computes the photon splitting probabilities and kinematics, while the principal user input commands to steer its behaviour are described in App. B. We will use the usual notation associated with a Catani-Seymour dipole shower, following [84]. Since the YFS algorithm requires massive charged particles, it is necessary to include all masses in this shower for consistency. There are therefore no infrared singularities associated with our photon splittings, since the collinear pole is regulated by the fermion and scalar masses. However, the aim is still to capture the correct behaviour in the quasi-collinear limit, accounting for the logarithmic enhancement for collinear splitting into light flavours. Throughout this section we will focus on configurations where all relevant particles are in the final state of the decay process, *i.e.* decays of neutral resonances. Decays of charged resonances are handled similarly; the corresponding modifications are detailed in App. A.

The key part of the parton shower algorithm is, as usual, the veto algorithm [85, 86]. This allows us to avoid the problem of analytically integrating the splitting functions, which are detailed below, by using an overestimate to evaluate the cumulative emission probability, and then vetoing emissions with a probability which corrects for the overestimate. The evolution begins at some starting scale t_{start} which is the highest possible scale for a splitting to take place; we postpone its exact definition to the end of this section. All splitting functions compete: a splitting scale is calculated for each possible combination of splitter \tilde{y} , splitting products i and j , and spectator \tilde{k}/k (before/after the splitting process). Whichever splitting process would happen at the highest scale is selected. If the splitting is accepted (not vetoed), a new particle is created and flavours and kinematics of existing particles are updated. The whole process is repeated, starting from the selected splitting scale, and iterated until some infrared cutoff t_0 is reached. This cutoff is needed to regulate the divergence of the splitting functions in the general case where these appear. For a QCD shower, a physical choice for the cutoff is the hadronisation scale, which is of $\mathcal{O}(1 \text{ GeV})$, well above Λ_{QCD} where QCD dynamics turn non-perturbative. For a QED shower, however, the splittings which do not involve quarks can evolve to arbitrarily low scales. In the algorithm presented here, which contains only splitting functions of photon emissions off charged scalars and fermions as well as of photons splitting into massive fermions or pseudo-scalar hadrons, the cutoff is dictated by the mass of the lightest fermion, $t_0 = 4m_e^2$ or lower.

As stated earlier, in the case of a photon splitting to a fermion or scalar particle-antiparticle pair, there is no soft divergence. The collinear divergence present for massless splitting products is converted into a logarithmic collinear enhancement when masses are included; hence, lighter particles will have a larger contribution to photon splitting corrections. Here we include all possible splittings up to a mass cutoff of $2m_i \lesssim 1 \text{ GeV}$ in addition to τ pair production which, while rare, contributes to some observables through the decays to lighter leptons or hadrons. Since most splittings occur near or below the hadronisation scale,

¹The hard (real and virtual) photon-emission corrections \mathcal{C} are available up to NLO EW for leptonic W decays and up to NNLO QED + NLO EW for leptonic Z decays [62].

we consider hadrons, not quarks, to be the relevant QCD degrees of freedom. Using this mass cutoff, the hadrons which can be produced are the charged pions and kaons. They are pseudo-scalars, and their interaction with photons is modeled using point-like scalar QED, neglecting any substructure effects. We use the scalar splitting functions of [87]. Depending on the experimental environment, the kaons and τ leptons decay before hitting any detector. This can be handled within the usual (hadron) decay treatment available within the SHERPA framework [59, 88].

Splitting functions and spectator assignment. In the usual parton shower notation, we use the following dipole splitting functions [87, 84, 89]

$$\begin{aligned}
S_{s_{\tilde{y}}(\tilde{k}) \rightarrow s_i \gamma_j(k)} &= S_{\bar{s}_{\tilde{y}}(\tilde{k}) \rightarrow \bar{s}_i \gamma_j(k)} = -\mathbf{Q}_{\tilde{y}\tilde{k}}^2 \alpha \left[\frac{2}{1-z+zy} - \frac{\tilde{v}_{\tilde{y},\tilde{k}}}{v_{ij,k}} \left(2 + \frac{m_i^2}{p_i p_j} \right) \right] \\
S_{f_{\tilde{y}}(\tilde{k}) \rightarrow f_i \gamma_j(k)} &= S_{\bar{f}_{\tilde{y}}(\tilde{k}) \rightarrow \bar{f}_i \gamma_j(k)} = -\mathbf{Q}_{\tilde{y}\tilde{k}}^2 \alpha \left[\frac{2}{1-z+zy} - \frac{\tilde{v}_{\tilde{y},\tilde{k}}}{v_{ij,k}} \left(1 + z + \frac{m_i^2}{p_i p_j} \right) \right] \\
S_{\gamma_{\tilde{y}}(\tilde{k}) \rightarrow s_i \bar{s}_j(k)} &= S_{\gamma_{\tilde{y}}(\tilde{k}) \rightarrow f_i \bar{f}_j(k)} = -\mathbf{Q}_{\tilde{y}\tilde{k}}^2 \alpha \left[1 - 2z(1-z) - z_+ z_- \right]
\end{aligned} \tag{2.2}$$

for splittings involving the scalars s , fermions f , their antiparticles \bar{s} and \bar{f} , and a photon γ , in terms of the splitting variable y and light-cone momentum fraction z . These are defined as

$$y = \frac{p_i p_j}{p_i p_j + p_i p_k + p_j p_k} \quad \text{and} \quad z = \frac{p_i p_k}{p_i p_k + p_j p_k} . \tag{2.3}$$

Further, m_i is the mass of the splitting product i , and z_- and z_+ are the phase space boundaries

$$z_{\pm} = \frac{2\mu_i^2 + (1 - \mu_i^2 - \mu_j^2 - \mu_k^2) y}{2(\mu_i^2 + \mu_j^2 + (1 - \mu_i^2 - \mu_j^2 - \mu_k^2) y)} (1 \pm v_{ij,i} v_{ij,k}) , \tag{2.4}$$

where the dimensionless rescaled masses $\mu_i^2 = m_i^2/Q^2$ are introduced for convenience, and $Q^2 = (p_i + p_j + p_k)^2 = (p_{\tilde{y}} + p_{\tilde{k}})^2$ is the invariant mass of the dipole. The relative velocities $\tilde{v}_{\tilde{y},\tilde{k}}$, $v_{ij,k}$, and $v_{ij,i}$ are given by

$$\begin{aligned}
\tilde{v}_{\tilde{y},\tilde{k}} &= \frac{\sqrt{\lambda(1, \mu_{\tilde{y}}^2, \mu_{\tilde{k}}^2)}}{1 - \mu_{\tilde{y}}^2 - \mu_{\tilde{k}}^2} , \\
v_{ij,i} &= \frac{\sqrt{(1 - \mu_i^2 - \mu_j^2 - \mu_k^2)^2 y^2 - 4\mu_i^2 \mu_j^2}}{(1 - \mu_i^2 - \mu_j^2 - \mu_k^2) y + 2\mu_i^2} , \\
v_{ij,k} &= \frac{\sqrt{(2\mu_k^2 + (1 - \mu_i^2 - \mu_j^2 - \mu_k^2)(1 - y))^2 - 4\mu_k^2}}{(1 - \mu_i^2 - \mu_j^2 - \mu_k^2)(1 - y)} .
\end{aligned} \tag{2.5}$$

Finally, the charge correlator $\mathbf{Q}_{\tilde{y}\tilde{k}}^2$ is defined as [52, 90, 91, 89]

$$\mathbf{Q}_{\tilde{y}\tilde{k}}^2 = \begin{cases} \frac{Q_{\tilde{y}} Q_{\tilde{k}} \theta_{\tilde{y}} \theta_{\tilde{k}}}{Q_{\tilde{y}}^2} & \tilde{y} \neq \gamma \\ \kappa_{\tilde{y}\tilde{k}} & \tilde{y} = \gamma \end{cases} \quad \text{with} \quad \sum_{\tilde{k} \neq \tilde{y}} \kappa_{\tilde{y}\tilde{k}} = -1 \quad \forall \tilde{y} = \gamma , \tag{2.6}$$

where the $Q_{\tilde{y}}$ and $Q_{\tilde{k}}$ are the charges of the splitter and spectator respectively and their $\theta_{\tilde{y}/\tilde{k}}$ are 1 (−1) if they are in the final (initial) state. The $\kappa_{\tilde{y}\tilde{k}}$ need to ensure that the splitting functions are appropriately normalised such that the correct collinear limit is found, but are otherwise unconstrained. Here we choose

$$\kappa_{\tilde{y}\tilde{k}} = -\frac{1}{\mathcal{N}_{\text{specs}}} , \tag{2.7}$$

where $\mathcal{N}_{\text{specs}}$ is the chosen number of possible spectators, *i.e.* we choose to weigh all selected spectators \tilde{k} equally. The photon splittings themselves are free of soft divergences, hence the spectator is only needed for momentum conservation and, in principle, any other particle of the process may assume this role. In the

present context, we consider all primary charged decay products as possible spectators of photon splittings as our default, but the choice to consider only the splitting photon's originator particle (as reconstructed, described below) has also been implemented, *see* App. B. While the other present YFS photons and other neutral decay products as well as the decaying particle itself are all valid spectators, the two choices described above both guarantee that enough energy is available to allow photon splitting into heavier flavours to occur. Limiting the number of spectators also helps to reduce the computational complexity. For photon radiation off the products of a photon splitting, the spectator assignment, and therefore the recoil, is kept local in that system.

Evolution variable. For the evolution variable t used in the parton shower, the requirement of leading logarithmic accuracy means that any choice which preserves dt/t is formally equivalent in the infrared limit. In a given splitting function we consider two variants, virtuality \bar{q}^2 and transverse momentum k_T^2 . The virtuality is defined, in terms of the dipole invariant mass Q^2 and the masses of the emitter $m_{\tilde{q}}$, splitting products $m_{i/j}$ and spectator m_k , as

$$\bar{q}^2 = (Q^2 - m_i^2 - m_j^2 - m_k^2) y + m_i^2 + m_j^2 - m_{\tilde{q}}^2. \quad (2.8)$$

Specifically, for the two relevant cases this translates to

$$\bar{q}_{\tilde{f} \rightarrow f \gamma}^2 = (Q^2 - m_f^2 - m_k^2) y \quad (2.9)$$

for photon emissions, where the flavour f can either be a scalar s , fermion f , or their antiparticles \bar{s} and \bar{f} , and

$$\bar{q}_{\gamma \rightarrow f \bar{f}}^2 = (Q^2 - 2m_f^2 - m_k^2) y + 2m_f^2 \quad (2.10)$$

for photon splittings. We see that, as stated earlier, photon emissions are possible at arbitrarily low evolution scales while photon splittings can only occur if the virtuality exceeds the pair-production threshold. Likewise, the transverse momentum is defined by [84]

$$k_T^2 = (Q^2 - m_i^2 - m_j^2 - m_k^2) y z(1-z) - m_i^2(1-z)^2 - m_j^2 z^2. \quad (2.11)$$

Again, for photon emissions this translates to

$$k_{T f \rightarrow f \gamma}^2 = (Q^2 - m_f^2 - m_k^2) y z(1-z) - m_f^2(1-z)^2 \quad (2.12)$$

and to

$$k_{T \gamma \rightarrow f \bar{f}}^2 = (Q^2 - 2m_f^2 - m_k^2) y z(1-z) - m_f^2(z^2 + (1-z)^2) \quad (2.13)$$

for photon splittings. As discussed, photon emissions are possible down to $k_T^2 = 0$, but in this case the photon-splitting threshold also lies at $k_T^2 = 0$. As a result, the chosen infrared cutoff t_0 will induce a minimal k_T , and thus opening angle, produced in the pair-creation process. Hence, in full analogy to most QCD parton showers, the pair's virtuality \bar{q}^2 , with its automatic introduction of a pair-production threshold, is expected to give a better description.

It can be seen that the relation

$$\frac{dt}{t} = \frac{dk_T^2}{k_T^2} = \frac{d\bar{q}^2}{\bar{q}^2} \quad (2.14)$$

holds, therefore both transverse momentum and virtuality are possible choices of evolution variable and no Jacobian is needed to translate between them.

Using these definitions, there are three well-motivated choices for the global evolution variable.

1. As in most QCD parton showers, $t = k_T^2$ is a viable choice. In analogy to QCD, ordering photon emissions by transverse momentum results in the inclusion of charge coherence effects [92], but there is no particular motivation to use $t = k_T^2$ as the evolution variable for photon splittings into charged-particle pairs.

2. Choosing $t = \bar{q}^2$ is an equally valid option. Due to the s -channel nature of photon splittings, the photon virtuality is expected to be a good ordering variable here [55, 93]. But since it does not implement angular ordering natively, it is not expected to yield the best description of soft-photon emissions.
3. Following eq. (2.14), we are free to interpret the evolution variable differently in different splitting processes as long as dt/t is invariant. As our default, we thus choose to interpret the evolution variable t as k_T^2 in photon emissions and as \bar{q}^2 in photon splittings. We will call this the “mixed scheme” in later sections.

All three choices are implemented, *see* App. B, and some of their respective consequences will be explored in Sec. 2.3.

Generation of splitting variables. While the evolution variable t is generated as usual in the veto algorithm, the light-cone momentum fraction z has to be generated within its allowed range $[z_-, z_+]$. The integration limits z_{\pm} are defined in eq. (2.4), but in order to generate a Sudakov factor we work with the evolution variable t . We generate a trial emission using the integral of the overestimate of the splitting function, for which the z limits are necessary, but we do not yet know the value of the kinematic variable y (eq. (2.3)). Using a change of variables to replace y with the evolution parameter yields usable z ranges at this stage. Hence in the k_T ordered scheme, the z limits are [84]

$$z_{\pm, k_T} = \min/\max \left[\frac{1}{2} \left(1 \pm \sqrt{1 - \frac{4t_0}{Q^2}} \right), z_{\pm} \right]. \quad (2.15)$$

Note that the z_{\pm} are not yet known, but can be overestimated by 0 and 1, respectively. The above expression thus gives an overestimate of the true phase space available. The number of splittings rejected as a result is very small, however, and does not have a large impact on the efficiency of the algorithm.

On the other hand, in the virtuality ordered scheme \bar{q}^2 has no z dependence. This means that y can be determined independently of the light-cone momentum fraction z as well, $y(t, z) = y(t)$, by solving eq. (2.8) for y . This implies that the z limits can be written as

$$z_{\pm, \bar{q}} = \min/\max \left[\frac{q^2 + m_i^2 - m_j^2}{2q^2} \left(1 \pm \sqrt{1 - \frac{4m_i^2 q^2}{(q^2 + m_i^2 - m_j^2)^2}} \sqrt{1 + \frac{4m_k^2 q^2}{(Q^2 - q^2 - m_k^2)^2}} \right), z_{\pm} \right] \quad (2.16)$$

where $q^2 = \bar{q}^2 + m_{\tilde{\gamma}}^2$. Again, however, it is only a small price in efficiency to use larger and simpler limits at the trial emission stage. In the results that follow, $z_{-, \bar{q}^2} = 0$ and $z_{+, \bar{q}^2} = 1$ have been used.

Kinematics. With the above definitions of the dipole variables y and z or, alternatively, with the evolution variable t and the splitting variable z , and the uniformly distributed azimuthal splitting angle ϕ , we can now build the kinematics of the splitting products i and j and the spectator k after the emission process. The new momenta are given by an inversion of the momentum maps of [87], and in their construction we follow [84]. In particular, for the final-final (FF) dipoles discussed here, they are given in Sec. 3.1.1 eq. (49)–(58) of [84]. Note that this redistribution of momenta is infrared safe and does not spoil the leading logarithmic accuracy of the YFS resummation, since it introduces non-logarithmic corrections only.

Starting conditions. Having defined the evolution and splitting variables as well as the splitting functions and kinematic mappings above, we now need to specify the initial conditions to fully define the algorithm. As the photon emissions are already generated by the YFS soft-photon resummation, the existing distribution has to be reinterpreted as if it was generated by our shower algorithm. Then, the missing photon-splitting corrections can be embedded into the existing calculation. By not allowing further photon-radiation off the primary charged-particle ensemble, double counting is avoided.

To determine the scale at which each existing photon has been produced, we calculate the emission probabilities according to the splitting functions $S_{f_{\tilde{\gamma}}(\tilde{k}) \rightarrow f_i \gamma_j(k)}$ and $S_{s_{\tilde{\gamma}}(\tilde{k}) \rightarrow s_i \gamma_j(k)}$, respectively, for every existing soft-photon γ_j . Therein, every primary charged particle (all existing charged particles of the process at the this stage) can act as possible emitter $\tilde{\gamma}$ and spectator \tilde{k} . One of those possible splitting functions is then selected either according to its probability $S_{\tilde{\gamma}\tilde{k} \rightarrow ij k} / \sum_{\tilde{\gamma}\tilde{k}} S$ (default), or by selecting the one with the

largest splitting probability (*see* App. B). Its reconstructed evolution variable t is then set as the starting scale $t_{\text{start},j}$ of the further evolution for photon γ_j . The above parton shower algorithm is then started at the largest of all photons' starting scale, $t_{\text{start}} = \max[t_{\text{start},j}]$, but each individual photon's evolution is only active for $t \leq t_{j,\text{start}}$.

2.3 Properties of the photon-splitting algorithm

Having the algorithm to calculate photon splitting probabilities at hand, we can now examine its properties and assess the consequences of specific algorithmic choices discussed above. To be precise, we use the example of an on-shell Z boson decaying to an e^+e^- pair (maximising the number of radiated photons). Hence, as we are not in a collider environment, we use a spherical coordinate system to measure relative radial distances $\Delta\Theta$ in the following.

We begin by presenting a detailed look into the conditions under which the photons generated through the YFS soft-photon resummation split. As discussed, in a first step, the existing distribution of photons and primary emitters has to be clustered to assign individual starting scales to the evolution of each photon. This assignment is of course dependent on the choice of evolution variable for photon emissions off charged particles as well as the choice of spectator scheme.

Fig. 1 shows the distribution of starting scales when the photon emissions are reconstructed with the inverse emission kernels. In the left plot, the ordering variable is interpreted as either a relative transverse momentum, $t = k_{\text{T}}^2$ (red) or a virtuality, $t = \bar{q}^2$ (blue). In the transverse momentum ordering scheme we observe an approximately logarithmic rise in the abundance of starting scales, starting at the kinematic limit of $k_{\text{T}}^2 \simeq \frac{1}{4} m_Z^2$. This reflects the photon spectrum produced by the soft-photon resummation. This logarithmic rise levels out at $k_{\text{T}}^2 \approx m_e^2$, formed by the reconstructed k_{T}^2 of ultra-soft photons of the event. This plateau ends at the soft-photon cutoff $\omega_{\text{IR,YFS}}^2$ used in the soft-photon resummation. In contrast, in the virtuality ordering scheme we see the majority of events have starting scales above 10^{-6} GeV. In both cases the characteristic scale at $t = m_e^2$ is induced by both the splitter and the spectator masses of the primary decay. The effect of the infrared cutoff is straightforward in the $t = k_{\text{T}}^2$ case, as shown by the labelled black dashed line. In the $t = \bar{q}^2$ case the cutoff does not dictate the turning point of the frequency plot, but, indirectly, the point at which the frequency falls to zero. Due to normalisation this has the effect of increasing the frequency above the electron mass. This appears as a flattening off of the plot just above the electron mass squared, before the frequency falls towards zero at m_Z^2 independent of the IR cutoff. We note that in the mixed ordering scheme, which we choose as our default ordering variable scheme, $t_{\text{start}} = k_{\text{T},\text{start}}^2$.

On its right-hand side, Fig. 1 shows the distribution of starting scales $t_{\text{start}} = k_{\text{T}}^2$ when the reconstructed emission of a YFS photon from one of the final-state charged particles is chosen either probabilistically according to the relative sizes of the splitting functions (red, our default) or by simply choosing the more likely emitter (green, dashed). There is no significant difference between the two schemes. A very small difference occurs at the high t_{start} end. In the winner-takes-all scheme, large starting scales are less likely because the emitter with the largest splitting function is always chosen; the chosen emitter is the particle which results in a smaller starting scale, due to the soft divergence and collinear enhancement of the splitting functions.

Having established the starting conditions of the photons' evolution we can now examine their splitting process into pairs of charged particles, and the interplay of the choice of interpretation of the evolution variable in either splitting process. Therefore, Fig. 2 depicts the correlation of the starting scale $t_{\text{start},j}$ of a photon and the collinearity, or opening angle $\Delta\Theta_{\text{pair}}$, of its splitting products (mainly e^+e^- pairs), for all three different choices of interpretation of the evolution variable t : \bar{q}^2 , k_{T}^2 , or mixed. In the virtuality-ordered scheme, $t = \bar{q}^2$, photons can only split if t exceeds the pair-creation threshold of the lightest charged species, $t \geq 4m_e^2 \approx 10^{-6}$ GeV². Further, there is also a strong correlation between the starting scale of the evolution and the eventual splitting angle, which is mainly a consequence of the identification of the starting scale t_{start} for each photon. As already anticipated in section 2.2 above, the evolution scale in the k_{T} -ordered case is only constrained to be above the infrared cutoff t_0 , which is also chosen to be $t_0 = 4m_e^2$ here. This constrains the opening angle of the pair of splitting products to be $\Delta\Theta_{\text{pair}} \gtrsim 10^{-4}$. The mixed scheme, interpreting $t = k_{\text{T}}^2$ in reconstructing the photon emission to define t_{start} and $t = \bar{q}^2$ in photon splittings, combines aspects of these two schemes, producing a smooth distribution in the whole $(t_{\text{start}}, \Delta\Theta_{\text{pair}})$ space independent of t_0 , as long as $t_0 \leq 4m_e^2$. The opening angle becomes relevant when studying the recombination properties of the splitting product into a dressed primary charged particle, *see* Sec. 3.1.

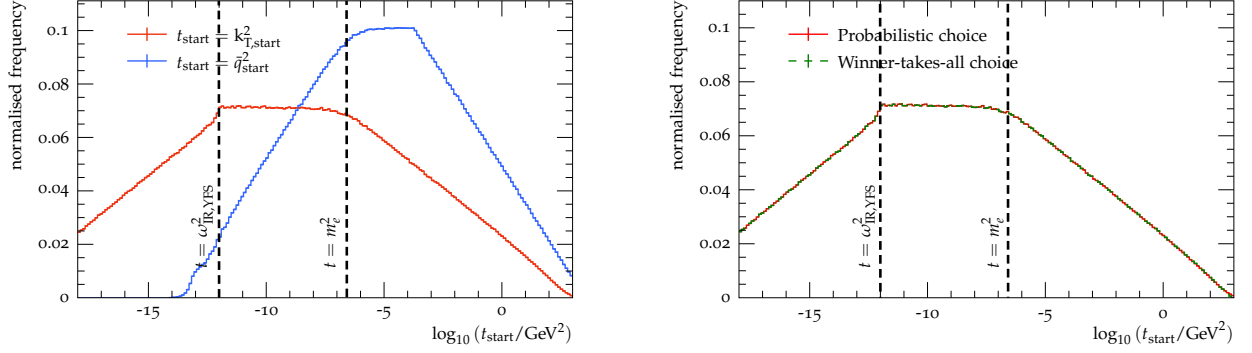


Figure 1: **Left:** A comparison of the frequency of the reconstructed starting scales t_{start} using two choices for the evolution variable t , k_{T}^2 or \bar{q}^2 , in the reconstructed initial $e^\pm \rightarrow e^\pm \gamma$ splitting. **Right:** A comparison of the frequency of the reconstructed starting scales $t_{\text{start}} = k_{\text{T},\text{start}}^2$ using either a probabilistic determination of the emitter lepton or a winner-takes-all in the reconstructed initial $e^\pm \rightarrow e^\pm \gamma$ splitting. The threshold for photons splitting into charged particle pairs is $t > 4m_e^2$, and $\omega_{\text{IR},\text{YFS}}^2$ is the infrared cutoff of the YFS-style algorithm which generates the photons.

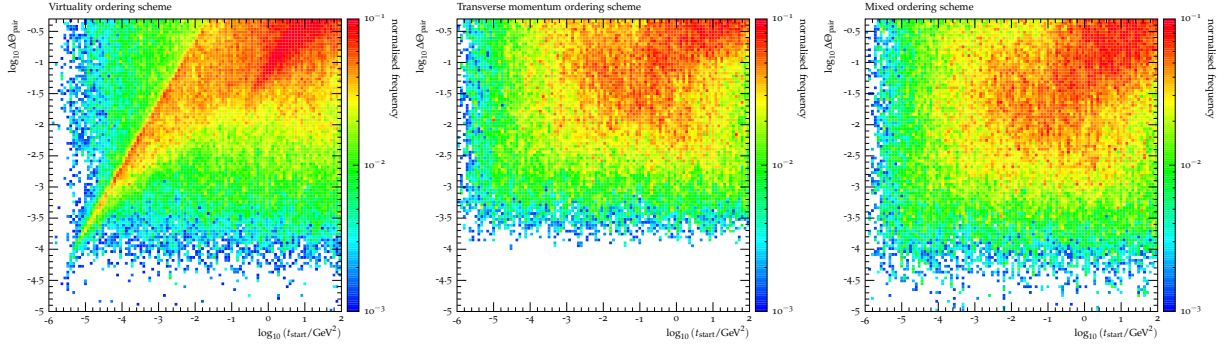


Figure 2: The interdependence of the starting scale t_{start} of a photon and the angular separation between the particles produced in its splitting, $\Delta\Theta_{\text{pair}}$, in the in the \bar{q} -ordered scheme (left), the k_{T} -ordered scheme (centre), and the mixed ordering scheme (right).

To further investigate the effects of our results on specific algorithmic choices, Fig. 3 focuses on the same observable familiar from the previous figure: the interdependence of the starting scale t_{start} and the opening angle $\Delta\Theta_{\text{pair}}$. Here as in Fig. 1, we see that the effect of a winner-takes-all choice of starting scale as opposed to our default probabilistic starting scale definition is not significant. The winner-takes-all choice results in the distribution of starting scales being skewed to slightly smaller values, as discussed above, which correlates loosely with a more collinear splitting. This results in a slight extension of the high-frequency (red) region of the plot towards the small- t_{start} small-angle corner in the lower two plots of Fig. 3 compared to the upper two plots. We also show the spectator scheme dependence in the photon splitting: whether we allow both primary leptons to be spectators or only the lepton that the photon was reconstructed to have been emitted from. Since in photon splittings, the spectator's only role is to absorb recoil to guarantee momentum conservation, it is physically well motivated for the splitting photon's progenitor to be the sole particle to absorb its gained virtuality necessary for the splitting process. Note that this choice does not affect the value of t_{start} , only the energy available in the splitting, which affects the overall splitting probability and the allowed opening angle of the splitting products. Fig. 3 shows that this choice has negligible effect on the distribution of splitting events in the $(t_{\text{start}}, \Delta\Theta_{\text{pair}})$ plane.

To conclude this section, Fig. 4 shows the relative frequency of photons splitting into different species of charged lepton and hadron. As the driving factor is the produced particle species' mass, electron-positron pairs are most commonly produced, around an order of magnitude more commonly the products of photon splittings than muons or charged pions. The probability of producing a second pair of a given species roughly follows the naïve expectation of being the square of the probability of producing one pair. In a more

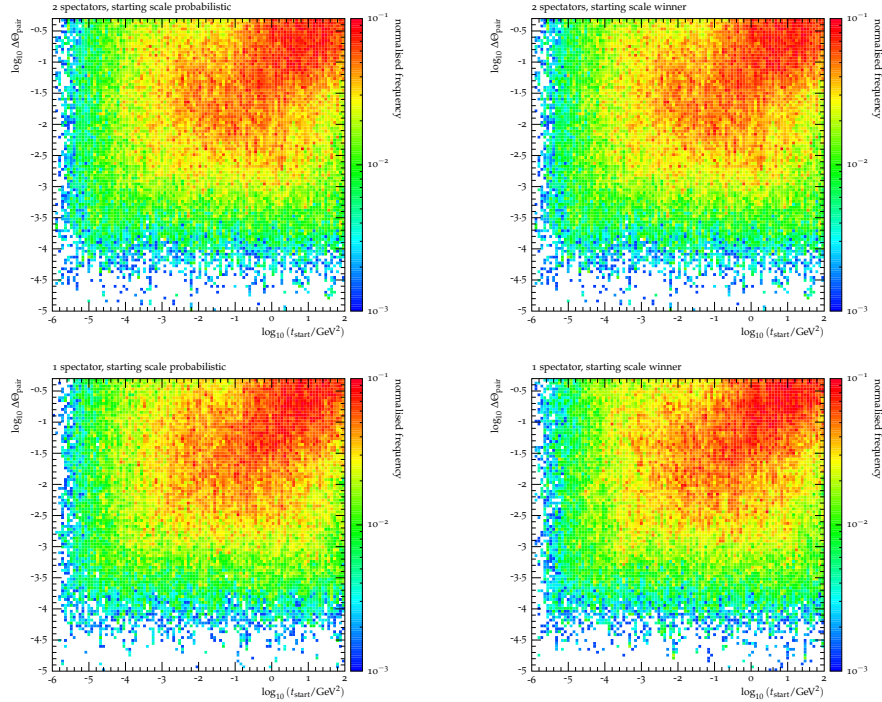


Figure 3: The interdependence of the starting scale t_{start} of a photon and the angular separation between the particles produced in its splitting, $\Delta\Theta_{\text{pair}}$, in mixed ordering scheme with different choices of kinematic spectators of the photon splitting, both charged primary leptons (top row) or only the primary lepton the splitting photon was reconstructed to have been emitted from (bottom row), and the way in which the starting scale of the evolution is chosen, probabilistically (left column) or by always choosing the winning dipole (right column).

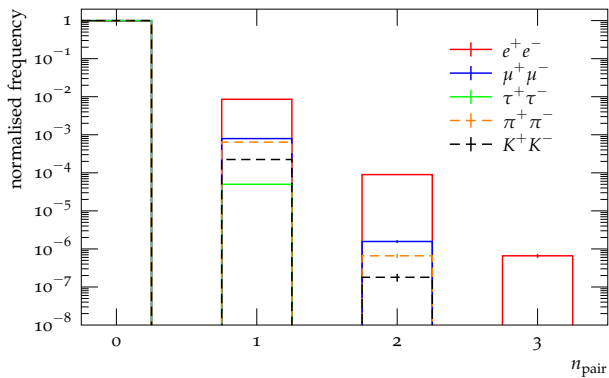


Figure 4: The relative abundance of secondary pairs of each species of charged particle produced in photon splittings in the mixed ordering scheme.

detailed consideration one finds a factor of $\alpha^2 \log(m_Z/E_\gamma) \log(t_{\text{start}}/m^2)$ associated with each secondary pair production. Therein, E_γ is the energy of the bremsstrahlung photon that subsequently splits into the pair of particles of mass m , and t_{start} is its reconstructed starting scale. Hence, we observe a single-logarithmic suppression of heavier flavours, modulo possible minor differences in the splitting function itself. This is well-reproduced by our algorithm. In fact, in the current example, the drop in frequency of producing an additional pair of particles of the same flavour is between 2.5 and 4.5 orders of magnitude.

3 Lepton dressing beyond photons

In this section we analyse the final states produced by our algorithm, and in particular the consequences of further resolving the photons produced by the standard soft-photon resummation into charged-particle pairs. We will continue to use the decay of an on-shell Z boson into an e^+e^- pair as a testbed for our algorithm. We will analyse the corrections induced by photon splittings on a number of physical properties that are related to the charged particle content of the radiation cloud surrounding the primary decay products.

The reader is reminded that we continue to use a spherical coordinate system to measure relative radial distances $\Delta\Theta$. Further, please note that for this study we turn off kaon and τ decays for the greatest accuracy in identifying primary final-state particles. By default, however, kaon and τ lepton decays would be handled as normal in SHERPA [59], including various state-of-the-art parametrisations of all known decay channels and including their own respective QED corrections.

3.1 Dressing strategies in the presence of photon splittings

Lepton dressing is commonly used to define infrared-safe observables through recombining a primary bare lepton with its surrounding radiation cloud, in full analogy with the jet clustering of QCD. While lepton dressing is essential when massless leptons are used in a calculation due to the presence of collinear singularities, the inclusion of a lepton mass renders both dressed and bare lepton definitions physical. Nonetheless, bare leptons suffer from large corrections that are logarithmic in the lepton's mass, making them particularly relevant for electrons. Hence, a dressed lepton definition is also advantageous in calculations with massive, but light, leptons.

In practice, there are two common methods for lepton dressing, analogous to jet definitions in QCD: cone dressing and sequential recombination dressing. While a sequential recombination algorithm typically uses either the anti- k_t or Cambridge-Aachen algorithm [94], the cone-based dressing uses the bare lepton to define the cone axis and, at variance with historical QCD cone algorithms, keeps the cone itself stable throughout the recombination procedure, rendering it collinear safe. In either case, the algorithm is not completely blind to particle flavour since (at least) the primary bare lepton is used as the dressing-initiator and defines the flavour of the resulting dressed lepton. As long as only photon radiation is considered as a higher-order correction to lepton production, which is the current standard in both YFS based soft-photon resummations [60, 61] and PHOTOS [76, 78], both algorithms work very straightforwardly by subsequently combining the primary lepton with the surrounding photon cloud using the respective distance measure.

When photon splittings are included in the QED corrections to lepton production as well, the radiation cloud surrounding the primary lepton becomes flavour-diverse. Considering the underlying physical process, these photon-splitting corrections are simply resolving the structure of the photons constituting the above photon cloud. While these corrections are infrared finite when all lepton masses are considered, large logarithmic effects can be expected in particular when branching into the lightest species, electrons, occurs. Further, the splitting into electrons is the most probable branching for a photon emitter. Thus, while continuing to dress the primary leptons with photons only is infrared safe, it is natural to demand that the resulting dressed lepton definition does not strongly depend on whether or not we include further photon splittings. We will thus investigate the following choices for the flavour set f_{dress} which is used to dress the primary lepton:

- $\{\gamma\}$ We continue to use only photons to dress the primary charged lepton.
- $\{\gamma, e\}$ In addition to the mandatory dressing with the surrounding photons, we also include the lightest charged particle, the electron, in the dressing procedure of the primary lepton. This is not only motivated by the fact that splittings into e^+e^- pairs give the largest corrections, but also that experimentally both electrons and photons are measured similarly in the calorimeter. Of course, the presence of a magnetic field between the interaction and the calorimeter does in principle decorrelate the direction of their respective momentum vectors.
- $\{\gamma, e, \pi, K\}$ We also include the lightest hadronic splitting products in the dressed lepton definition. Such a definition is a compromise between theoretical inclusivity and experimental feasibility.
- $\{\gamma, e, \pi, K, \mu, \tau\}$ We include all species produced in our photon-splitting implementation in order to be completely inclusive. It has to be noted though, that in realistic

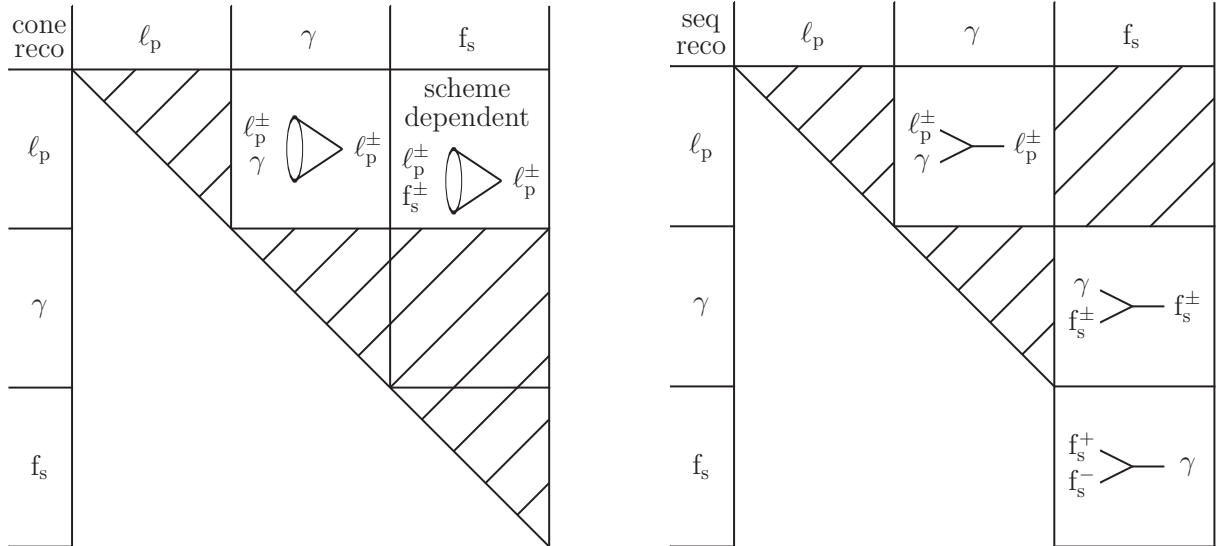


Figure 5: Recombination matrices of lepton dressing strategies beyond photon radiation. While γ labels the photon, l_p and f_s denote the primary leptons and secondary flavours, respectively.

experimental environments muons are well distinguishable even at low muon energies, and τ leptons of course decay further before detection rendering their inclusion in any realistic dressing algorithm highly non-trivial.

A schematic of how both the cone and sequential recombination dressing algorithms in the presence of photon splittings proceed is given in Fig. 5. In the case of the case of cone dressing, the primary leptons should be identified, and should be dressed with all QED radiation that surrounds them, including other leptons and hadrons. In particular, the flavour of the dressed lepton does not change even if flavours other than a photon are included in it as it is determined entirely by the primary lepton. Thus, in consequence, the cone-dressed lepton may have a net charge that is different from that of its assigned flavour when not all photon-splitting products are recombined into the same dressed lepton. We will use this algorithm for the remainder of this study.

Nonetheless, a diagram of a flavour recombination matrix for sequential recombination dressing is shown on the right-hand side of Fig. 5. Here it is possible to recombine a secondary (and hence soft/collinear) lepton-antilepton pair into a photon, while allowing for even softer or more collinear surrounding photons to be combined with these charged leptons first. On the level of primary leptons, then, they are only dressed with photons, either from the final state or from previous secondary-lepton clusterings. This has the obvious advantage that the charge and flavour of the primary lepton matches that of the dressed lepton. It, however, is schematically more intricate and does not always lead circular dressed leptons, which are favoured experimentally, and the investigation is left to a future study.

The first observables we examine offer closer looks into the substructure of the cone-dressed leptons produced by different dressing strategies. Here and in the following we use the notation: either photon splittings to charged flavours f are present ($\gamma \rightarrow f\bar{f}$) or they are not (no $\gamma \rightarrow f\bar{f}$); the dressing algorithm is specified by the set of particle flavours f_{dress} which are included in the dressing.

The left-hand side plot of Fig. 6 displays the angular distance $\Delta\Theta$ of the cone-dressed lepton constituent from the primary lepton. To ensure infrared safety, only photons with $E_\gamma > 0.1 \text{ MeV}$ are included. A cutoff just below the electron mass has been selected to ensure that all electrons are included in the analysis. Besides observing the primary lepton's dead cone for $\Delta\Theta \lesssim 2 \cdot 10^{-5}$, we find that for $\Delta\Theta \lesssim 10^{-4}$ the constituent multiplicity when including photon splittings, irrespective of the dressing scheme used, coincides with the multiplicity when omitting such splitting. This corroborates our earlier expectation that collinear photons largely lack the necessary virtuality to split into a charged-particle pair. At larger angles, where the required virtuality can be more easily gained, a photon's probability to split increases. In consequence, when including photon-splitting effects in the calculation, but not accounting for the splitting products in the dressing, a drop in multiplicity can be observed. Including electrons as well as photons in the dressing

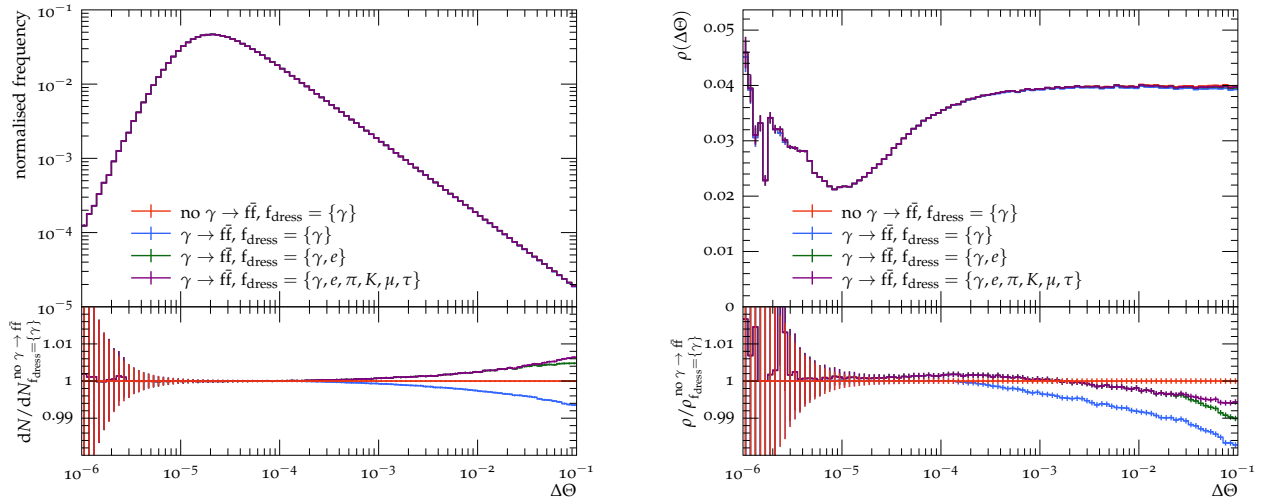


Figure 6: Left: The differential distribution of the dressed lepton constituents, including radiated photons with $E_\gamma > 0.1$ MeV, in dependence on the angular distance $\Delta\Theta$ from the primary lepton. **Right:** The energy density ρ within the dressed lepton as a function of the angular distance $\Delta\Theta$ from the primary lepton. Shown are the predictions without accounting for photon splittings (red), compared to the predictions allowing photons to split: dressed with photons only (blue), photons and electrons (green) or all particles (violet).

reincorporates most splitting products into the dressed lepton definition (*see* Fig. 4). We find an increase above the reference of approximately the same number of constituents that are lost in the $\gamma \rightarrow f\bar{f}$, $f_{\text{dress}} = \{\gamma\}$ (blue) case. The completely flavour-inclusive dressing definition then shows the same effects scaled to the production of heavier secondary species: larger virtualities, and thus larger $\Delta\Theta$, are needed for a non-zero splitting probability, so fewer photons actually split into these heavier flavours. This leads to a much smaller effect of these splittings, concentrated at the outside of the cone. We expect out-of-cone effects to be small, since the frequency spectrum falls steeply towards the edge of the cone. More generally, it appears that the splitting products are close to collinear with the progenitor photon, at least on average.

On the other hand, the right-hand side plot of Fig. 6 shows the distribution of energy within the dressed lepton as a fraction of the energy of the entire dressed lepton. Resolving photons into other species, *i.e.* pairs of charged particles, but continuing to dress the primary lepton with photons only, naturally decreases the energy radial density of the dressed lepton. The fact that this energy density loss is not constant but rather increases with the radial distance to the primary lepton is again a result of the increasing possible off-shellness at larger $\Delta\Theta$, and therefore the increased splitting probability. Even when the photon splittings products are part of the dressing procedure, either secondary electrons only or the set $\{e, \pi, K, \mu, \tau\}$, the energy density ρ falls below the reference at some distance from the primary lepton showing that a significant number of splitting products end up outside the dressing cone radius.

As mentioned above, it is possible for the charge of the dressed lepton to be different from the charge of its primary constituent. This is shown in Fig. 7 for the case of cone dressing with $\Delta\Theta_{\text{dress}} = 0.1$. Fewer than a thousandth of the dressed leptons are neutral or doubly charged, while a fraction of 10^{-7} of them are either triply charged or appear to be their own antiparticle (a dressed electron having a charge of +1 or a dressed positron having a charge of -1). Again, this is a consequence of only partially capturing the photon splitting products.

In the next section we will look at the separate and combined effects of photon splittings and flavour-aware lepton dressing on physical observables in the decay of an on-shell Z boson.

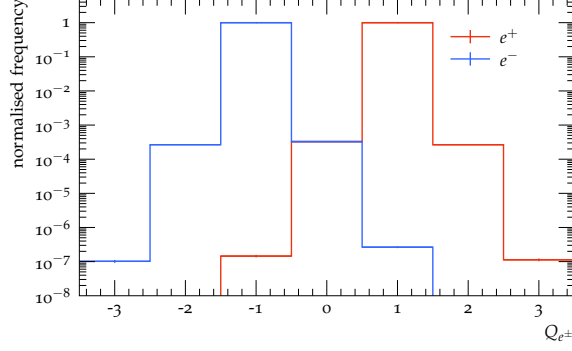


Figure 7: The total charge of the cone-dressed electron and positron with $\Delta\Theta_{\text{dress}} = 0.1$ and including all secondary flavours, *i.e.* $f_{\text{dress}} = \{\gamma, e, \pi, K, \mu, \tau\}$.

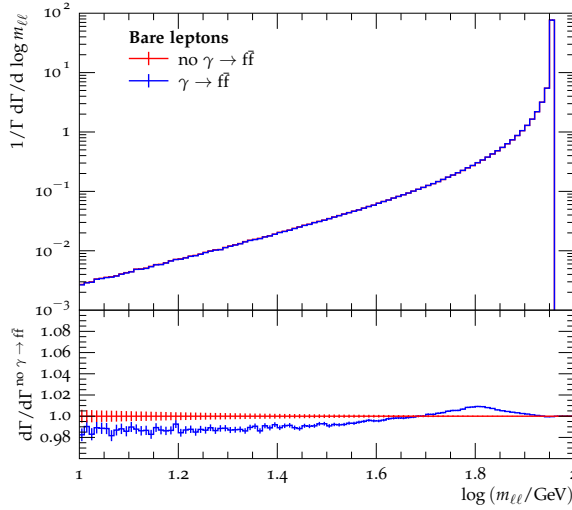


Figure 8: The bare dilepton invariant mass $m_{\ell\ell}$ as described by the YFS soft-photon resummation only (red) or additionally resolving the photons further into pairs of charged particles (blue), in the mixed ordering scheme.

3.2 Case study: Z boson decay

In a final step, we look at the decay of an on-shell Z boson into an e^+e^- pair and investigate the impact of the photon splitting corrections introduced in this paper on physical observables. To be precise, we present the effects of including $\gamma \rightarrow ff$ splittings and the consequences of (not) using flavour-aware dressing algorithms on the decay rate, differential with respect to the invariant mass $m_{\ell\ell}$ of the primary electron-positron pair.

We begin by examining the bare differential decay rate, *i.e.* the invariant mass of the primary lepton pair that is not dressed with the radiation around it, in order to quantify the kinematic effect of photon splittings on the primary leptons themselves without confusing this effect with the intricacies of the dressing algorithm. We note that bare leptons are theoretically well defined as all lepton masses are fully accounted for. To this end, Fig. 8 isolates the effect of allowing YFS photons to split by presenting the bare invariant mass of the two most energetic leptons of opposite charge, one electron and one positron. In the overwhelming majority of cases these are expected to be the primary electron-positron pair generated in the on-shell Z decay. The largest deviation from the pure YFS prediction without photon splittings, which is taken as the reference, is about 1% in the region of most interest. It occurs just below the Z mass, at about 60 – 70 GeV. It is driven by extracting additional momentum from the primary leptons to accommodate the necessary virtuality for photon splittings to occur. Although barely visible, this is fueled by a minute reduction of the much larger differential decay rate closer to the nominal Z mass itself. Although of less interest due to the smaller absolute decay rate, the opposite effect is seen at very small invariant masses, below 50 GeV, where,

through the same mechanism, the decay rate is diminished by about 1 – 2% as the slope of the distribution is shallower but the momentum extraction is similar in magnitude to that at larger invariant masses.

Finally, a change of the precise definition of the ordering variable, both for the reconstructed starting scale of the evolution and the splitting scale of the eventual photon splitting, generally increases the size of the corrections for this observable. While using $t = k_{\text{T}}^2$ for all splittings only increases the observed corrections slightly, due to the increased photon splitting probability as $k_{\text{T}} < \bar{q}$ throughout, using $t = \bar{q}^2$ almost doubles the size of the corrections as now the starting scales of the each photon’s evolution reconstruct to much larger values, *see* Fig. 1. This is a consequence of the different properties of these ordering variables as discussed in section 2.2, although *a priori* all choices have the same formal accuracy.

Having assessed the basic kinematic effects on the bare primary leptons, we now turn to dressed leptons. We will investigate the impact the different dressing strategies discussed in Sec. 3.1 have once the radiation cloud around the primary leptons is not comprised of only photons but is resolved further into various different flavours of secondary charged particles. To this end, Fig. 9 contrasts the pure YFS soft-photon resummation without further photon splittings with a range of dressing strategies when photon splittings are included. Four different cone sizes are considered, from $\Delta\Theta_{\text{dress}} = 0.005$ to $\Delta\Theta_{\text{dress}} = 0.2$. The upper ratio illustrates the deviation of each prediction from the pure YFS case, due to both the presence of photon splittings and the details of the dressing algorithm. The lower ratio isolates the effect of the dressing strategy by showing the deviation with respect to the photon-only-dressed events. In particular, this shows which secondary flavours are recombined with the primary lepton into the dressed lepton. We observe that when the photon radiation off the primary electrons is further resolved into charged-particle pairs but the primary electrons are still only dressed with only the photons of their surrounding radiation cloud, large effects are manifest. They range from slightly over 2% for $\Delta\Theta_{\text{dress}} = 0.005$ to 6% for the common $\Delta\Theta_{\text{dress}} = 0.1$, and up to 9% for the more inclusive cone radius of $\Delta\Theta_{\text{dress}} = 0.2$. This difference originates in the fact that as long as only photons are included in the dressing, every photon lost by resolving it into a charged-particle pair cannot be recombined into the dressed lepton, which then ends up with less energy simply because higher-order corrections have been included. The observation that our algorithm reconstructs higher starting scales for hard wide-angle photons than either soft or collinear ones, and thus these are more likely to possess the necessary virtuality to split into charged-particle pairs, explains the dressing-cone-size dependence. However, when more inclusive dressing algorithms are considered, the effect of photon splittings on the differential decay rate is reduced, as is the $\Delta\Theta_{\text{dress}}$ dependence. As photons predominantly resolve into e^+e^- pairs, their inclusion in the dressed lepton definition already captures the bulk of the effect, in particular at smaller dressing cone radii. Along the lines of the above argument, photons need to be sufficiently separated from the primary lepton in order to gain enough virtuality to split into the heavier particle species. Thus, the inclusion of further secondary flavours in the dressing algorithm only plays a role at larger dressing cones, with effects ranging from 1% at $\Delta\Theta_{\text{dress}} = 0.1$ to 2% at $\Delta\Theta_{\text{dress}} = 0.2$. The effect of changing the ordering scheme for the photon splitting algorithm on Fig. 9 is very similar to the effect on Fig. 8. Again, using the transverse momentum or virtuality ordered schemes increases the size of the corrections induced by photon splittings in a very similar way as before. It is still the case that reincorporating splitting products in the dressing recovers the bare-lepton level deviation from the pure YFS prediction. As above, it needs to be noted that such a change in the ordering variable results in a suboptimal description of the physical process, and is thus not recommended to be used as an estimator of the intrinsic uncertainty.

In Fig. 10 we show more clearly the recovery of the pure soft-photon prediction using the two most relevant charged-particle-inclusive dressing strategies. The figure shows the ratio of the differential cross section including photon splittings to that without photon splittings for different dressing choices. We find that including charged particles in the cone dressing limits the effect of photons splitting corrections to the 1% level, irrespective of cone size. Including electrons in the dressing similarly limits the corrections to 2% even for the largest cone sizes considered here.

4 Conclusions

In this paper we detailed an extension to the soft-photon resummation in the Yennie-Frautschi-Suura framework to incorporate higher QED corrections originating in photon splittings into charged-particle pairs. These photon-splitting corrections, which resolve the substructure of the newly produced photons, are often larger than suggested by the formal accuracy. In particular, they can be logarithmically enhanced with the ratio of the lightest charged particle, the electron, to the possible virtuality of the splitting photon.

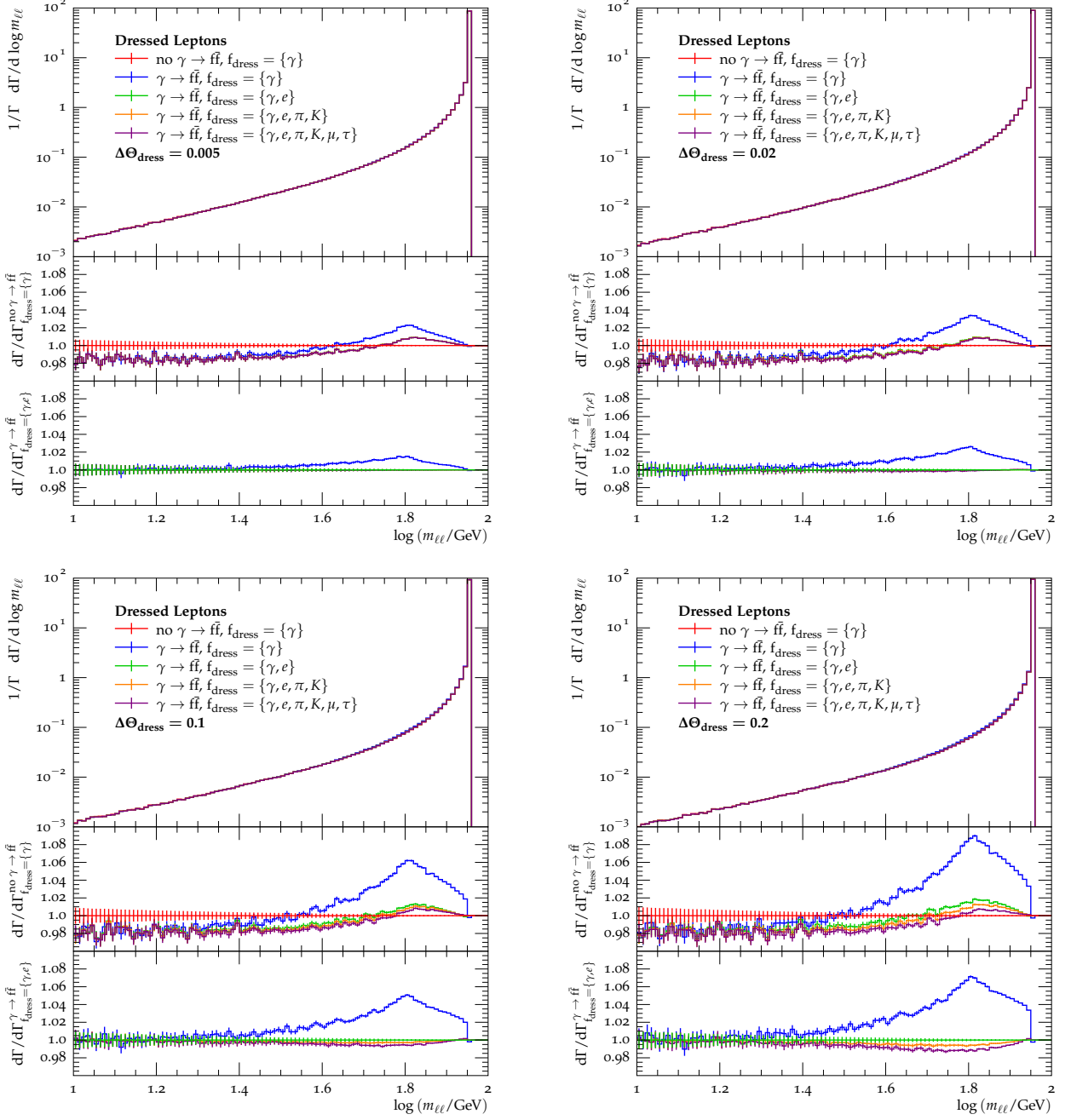


Figure 9: The dressed dilepton invariant mass $m_{\ell\ell}$ as described by the YFS soft-photon resummation only (red) or additionally resolving the photons further into pairs of charged particles for four different dressing cone sizes, $\Delta\Theta_{\text{dress}} = 0.005$ (top left), 0.02 (top right), 0.1 (bottom left), and 0.2 (bottom right), in the mixed ordering scheme. We differentiate various different dressing strategies, recombining photons only (blue), photons and electrons (green), photons, electrons and charged hadrons (orange), and all charged particles (violet) within the dressing cone with the primary charged lepton. Two ratios are presented, either taking the soft-photon resummation without photon splittings (upper ratio), or the soft-photon resummation including photon splittings and dressing the primary leptons with photons as well as secondary electrons (lower ratio), as the reference.

Using the decay $Z \rightarrow e^+e^-$, we found that that the limit on the virtuality of the photon bremsstrahlung off a primary lepton is strongly correlated with the angular distance to this primary lepton, and thus also to the

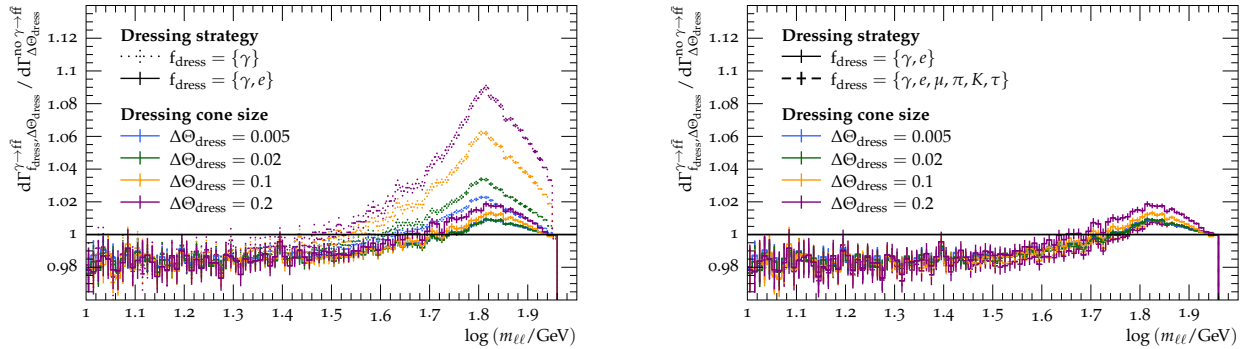


Figure 10: This figure shows the cone size dependence of different dressing strategies. The differential decay rate $d\Gamma_{f_{\text{dress}}, \Delta\Theta_{\text{dress}}}^{\gamma \rightarrow \text{ff}} / d \log m_{\ell\ell}$ has been divided by the corresponding $d\Gamma_{\Delta\Theta_{\text{dress}}}^{\text{no } \gamma \rightarrow \text{ff}} / d \log m_{\ell\ell}$, in dependence of both the flavour set f_{dress} included in the dressing and the dressing cone of size $\Delta\Theta_{\text{dress}}$. The **left** plot shows the difference case where only photons are used in the dressing (dotted) and using both photons and secondary electrons (solid), whereas the **right** plot shows the difference between a dressing strategy using only photons and electrons (solid) and all secondary flavours (dashed).

probability of that photon to split. We also investigated the systematics of our photon-splitting algorithm and found that algorithmic choices do not have a large impact on results. We found that the frequency of occurrence of different species agreed with theoretical expectations, showing a logarithmic dependence on the mass of the produced particles.

As a consequence of our extension, the cloud of QED radiation surrounding the primary leptons of a hard decay contains an array of particle flavours, not solely photons. Hence, the standard dressing algorithms to define infrared-safe dressed leptons were found to develop a strong sensitivity to further resolving the initial soft-photon cloud, in particular for larger dressing-cone radii. We therefore developed a novel set of flavour-aware strategies for dressing charged leptons and investigated their respective properties. We found that including secondary electrons as a minimal addition in the dressing procedure already substantially reduces this dependence on photon resolution, while an inclusion of all possible secondary flavours minimises it.

Using the example of the $Z \rightarrow e^+e^-$ decay rate, we investigated the dilepton invariant mass in detail. We found corrections of around 1% from photon splittings, wrt. the previous standard of not further resolving the initial photon radiation on the bare electrons. In the more relevant case of leptons cone-dressed with photons only, these could become much larger, up to 9% for large dressing cone radii of $\Delta\Theta_{\text{dress}} = 0.1$ or 0.2 . Introducing a flavour-aware dressing algorithm restored the bare result to a large degree, however, reigning in the photon-splitting corrections to 1 – 2%, along with mostly removing their cone-size dependence. We leave it to a future publication to study how the above effects translate to the general off-shell production of a Drell-Yan lepton pair at a hadron collider.

The photon splitting corrections were implemented in the SHERPA Monte-Carlo event generator and will be incorporated in a future release. All analyses and dressing strategies were implemented using RIVET’s analysis tools [95, 96].

Acknowledgements

LF would like to thank Hitham Hassan for valuable discussions on this topic. MS is funded by the Royal Society through a University Research Fellowship (URF\R1\180549) and Enhancement Awards (RF\ERE\210397, RGF\EA\181033 and CEC19\100349). LF is supported by the UK Science and Technology Facilities Council under contract ST/T001011/1.

A Charged resonances

In this appendix we give the definitions for final-initial (FI) dipoles needed for the description of photon splittings in the QED corrections of charged particle decays, like $W \rightarrow \ell\nu$.

The notation used in this appendix is for the most part consistent with Sec. 2.2. We consider a charged resonance \tilde{a} (a) decaying to a charged particle \tilde{i} (i) and a recoiling system $\{\tilde{n}\}$ ($\{n\}$): $\tilde{a} \rightarrow \tilde{i}\{\tilde{n}\}$ before and $a \rightarrow i\{n\}$ after the emission of a photon j , respectively. Ordinarily the recoil from the splitting would be absorbed locally by either the spectator a when i is the emitter, or vice versa. Since a is the decaying particle, however, we have chosen to keep its momentum unchanged and redistribute the recoil effectively to the particle(s) $\{n\}$. This allows to use a single momentum map for both situations and combine both emitter-spectator designations into a single dipole splitting function. This not only simplifies its description, but also removes problems with the positivity of the partial-fractioned Catani-Seymour splitting functions in situations where the mass correction is larger than the (quasi-)collinear emission term. Hence, we follow the treatment in [97, 98] to construct the splitting functions and kinematic variables.

As described in Sec. 2, the first step in the photon splitting algorithm is to determine the starting scale of each photon by reconstructing its emission history. In principle, emission of a photon can occur from the decaying particle \tilde{a} or from its charged decay product \tilde{i} . However, since the former splitting is suppressed by the decaying particle's mass, it is much more likely to act as spectator. Instead, as discussed above, we employ a single splitting function which contains the initial-state emission term in addition to the final-state emission. As a consequence, in the soft limit the full eikonal is recovered and the dipole radiates coherently, but splitting from the initial-state particle is never kinematically considered when building the required single-emitter history in the collinear interpretation of our parton shower.

After calculating the starting scale, the photons' evolution begins and photon splittings are considered. Since a photon is never considered to be emitted from the initial-state charged particle, and the decaying particle has a restricted phase space for absorbing recoil in any case, the spectator in all photon splittings is chosen to be the final-state particle i . For this reason, we do not need the kinematic mappings for an FI dipole. The splitting function and evolution variable definitions are detailed below.

Splitting functions. The dipole invariant mass Q^2 is defined as

$$Q^2 = (\tilde{p}_{\tilde{i}\tilde{j}} - \tilde{p}_{\tilde{a}})^2 = (p_i + p_j - p_a)^2 \quad (\text{A.1})$$

for the case of a dipole with final-state emitter i and initial-state spectator a .

For convenience, we define the quantity

$$\bar{Q}^2 = m_a^2 - m_i^2 - m_j^2 - Q^2. \quad (\text{A.2})$$

The kinematic variables z and y are defined differently from the FF case; they are given by

$$y = \frac{p_i p_j}{p_a p_i + p_a p_j - p_i p_j - 2m_i^2 - 2m_j^2} \quad \text{and} \quad z = \frac{p_i p_a - p_i p_j - m_i^2}{p_i p_a + p_j p_a - 2p_i p_j - m_i^2 - m_j^2}. \quad (\text{A.3})$$

In terms of these variables the splitting functions are given by

$$\begin{aligned} S_{f_{\tilde{i}\tilde{j}}(\tilde{a}) \rightarrow f_i \gamma_j(a)} &= S_{\bar{f}_{\tilde{i}\tilde{j}}(\tilde{a}) \rightarrow \bar{f}_i \gamma_j(a)} = -\mathbf{Q}_{\tilde{i}\tilde{j}\tilde{a}}^2 \alpha \left[\frac{2}{1-z(1-y)} \left(1 + \frac{2m_i^2}{\bar{Q}^2} \right) - (1+z) - \frac{m_i^2}{p_i p_j} \right. \\ &\quad \left. - \frac{(p_i p_j)}{\bar{Q}^2} \frac{m_a^2}{\bar{Q}^2} \frac{4}{[1-z(1-y)]^2} \right], \\ S_{s_{\tilde{i}\tilde{j}}(\tilde{a}) \rightarrow s_i \gamma_j(a)} &= S_{\bar{s}_{\tilde{i}\tilde{j}}(\tilde{a}) \rightarrow \bar{s}_i \gamma_j(a)} = -\mathbf{Q}_{\tilde{i}\tilde{j}\tilde{a}}^2 \alpha \left[\frac{2}{1-z(1-y)} \left(1 + \frac{2m_i^2}{\bar{Q}^2} \right) - 2 - \frac{m_i^2}{p_i p_j} \right. \\ &\quad \left. - \frac{(p_i p_j)}{\bar{Q}^2} \frac{m_a^2}{\bar{Q}^2} \frac{4}{[1-z(1-y)]^2} \right]. \end{aligned} \quad (\text{A.4})$$

The additional factor $(1 + 2m_i^2/\bar{Q}^2)$ is needed to recover the soft eikonal limit by cancelling some of the mass dependence of the variables z and y . Note that $m_j = 0$ needs to be taken for the soft limit so is not present in this additional factor.

Evolution variable. As before, we consider two choices of evolution variable, virtuality and transverse momentum. The form of these variables in terms of the dipole invariant mass Q^2 and the masses of the particles in the process are very similar to those for FF dipoles.

The virtuality is given by

$$\bar{q}^2 = (m_a^2 - m_i^2 - m_j^2 - Q^2) y + m_i^2 + m_j^2 - m_{ij}^2 \quad (\text{A.5})$$

while the transverse momentum can be written

$$k_{\perp}^2 = (m_a^2 - m_i^2 - m_j^2 - Q^2) y z(1-z) - m_i^2(1-z)^2 - m_j^2 z^2. \quad (\text{A.6})$$

As before, the default scheme for the evolution variable is the mixed scheme, where the transverse momentum is computed as the starting scale for photon evolution but is interpreted as a virtuality thereafter. The pure transverse momentum and virtuality schemes are implemented as well.

B Usage

In this appendix we list the available keywords and settings in order to effect the various algorithmic choices described in this paper. They are

`YFS_PHOTON_SPLITTER_MODE` This setting governs which secondary flavours will be considered.

- 0 photons do not split,
- 1 photons split into electron-positron pairs,
- 2 muons,
- 4 tau leptons,
- 8 and/or light hadrons (up to `YFS_PHOTON_SPLITTER_MAX_HADMASS`).

The settings are additive, the default is 15.

`YFS_PHOTON_SPLITTER_MAX_HADMASS` This setting sets the mass of the heaviest hadron which can be produced in photon splittings. Note that vector splitting functions are not currently implemented. Default is 0.5 GeV.

`YFS_PHOTON_SPLITTER_ORDERING_SCHEME` This setting defines the ordering scheme used.

- 0 transverse momentum ordering,
- 1 virtuality ordering,
- 2 mixed scheme (default).

`YFS_PHOTON_SPLITTER_SPECTATOR_SCHEME` This setting defines the allowed spectators for the photon splitting process.

- 0 all primary emitters may act as spectator (default),
- 1 only the photon's reconstructed emitter is eligible as a spectator.

`YFS_PHOTON_SPLITTER_STARTING_SCALE_SCHEME` This setting governs the determination of the starting scale.

- 0 starting scale is chosen probabilistically (default),
- 1 the starting scale is chosen using a winner-takes-all strategy.

References

- [1] T. Aaltonen et al., CDF, *High-precision measurement of the W boson mass with the CDF II detector*, Science **376** (2022), no. 6589, 170–176, FERMILAB-PUB-22-254-PPD.
- [2] R. L. Workman et al., Particle Data Group, *Review of Particle Physics*, PTEP **2022** (2022), 083C01.
- [3] R. Aaij et al., LHCb, *Measurement of the W boson mass*, JHEP **01** (2022), 036, [arXiv:2109.01113 [hep-ex]].
- [4] M. Aaboud et al., ATLAS, *Measurement of the W-boson mass in pp collisions at $\sqrt{s} = 7$ TeV with the ATLAS detector*, Eur. Phys. J. C **78** (2018), no. 2, 110, [arXiv:1701.07240 [hep-ex]], [Erratum: Eur.Phys.J.C 78, 898 (2018)].
- [5] T. A. Aaltonen et al., CDF, D0, *Combination of CDF and D0 W-Boson Mass Measurements*, Phys. Rev. D **88** (2013), no. 5, 052018, [arXiv:1307.7627 [hep-ex]].
- [6] T. A. Aaltonen et al., CDF, *Precise Measurement of the W -Boson Mass with the Collider Detector at Fermilab*, Phys. Rev. D **89** (2014), no. 7, 072003, [arXiv:1311.0894 [hep-ex]].
- [7] V. M. Abazov et al., D0, *Measurement of the W Boson Mass with the D0 Detector*, Phys. Rev. Lett. **108** (2012), 151804, [arXiv:1203.0293 [hep-ex]].
- [8] T. Aaltonen et al., CDF, *Precise measurement of the W-boson mass with the CDF II detector*, Phys. Rev. Lett. **108** (2012), 151803, [arXiv:1203.0275 [hep-ex]].
- [9] V. M. Abazov et al., D0, *Measurement of the W boson mass*, Phys. Rev. Lett. **103** (2009), 141801, [arXiv:0908.0766 [hep-ex]].
- [10] T. Aaltonen et al., CDF, *First Run II Measurement of the W Boson Mass*, Phys. Rev. D **77** (2008), 112001, [arXiv:0708.3642 [hep-ex]].
- [11] T. Aaltonen et al., CDF, *First measurement of the W boson mass in Run II of the Tevatron*, Phys. Rev. Lett. **99** (2007), 151801, [arXiv:0707.0085 [hep-ex]].
- [12] V. M. Abazov et al., CDF, D0, *Combination of CDF and D0 Results on W Boson Mass and Width*, Phys. Rev. D **70** (2004), 092008, [hep-ex/0311039].
- [13] T. Affolder et al., CDF, *Measurement of the W boson mass with the Collider Detector at Fermilab*, Phys. Rev. D **64** (2001), 052001, [hep-ex/0007044].
- [14] V. M. Abazov et al., D0, *Improved W Boson Mass Measurement with the D0 Detector*, Phys. Rev. D **66** (2002), 012001, [hep-ex/0204014].
- [15] B. Abbott et al., D0, *A measurement of the W boson mass using electrons at large rapidities*, Phys. Rev. Lett. **84** (2000), 222–227, [hep-ex/9909030].
- [16] B. Abbott et al., D0, *A measurement of the W boson mass using large rapidity electrons*, Phys. Rev. D **62** (2000), 092006, [hep-ex/9908057].
- [17] J. Abdallah et al., DELPHI, *Measurement of the Mass and Width of the W Boson in e^+e^- Collisions at $\sqrt{s} = 161\text{-GeV} - 209\text{-GeV}$* , Eur. Phys. J. C **55** (2008), 1–38, [arXiv:0803.2534 [hep-ex]].
- [18] S. Schael et al., ALEPH, *Measurement of the W boson mass and width in e^+e^- collisions at LEP*, Eur. Phys. J. C **47** (2006), 309–335, [hep-ex/0605011].
- [19] P. Achard et al., L3, *Measurement of the mass and the width of the W boson at LEP*, Eur. Phys. J. C **45** (2006), 569–587, [hep-ex/0511049].
- [20] G. Abbiendi et al., OPAL, *Measurement of the mass and width of the W boson*, Eur. Phys. J. C **45** (2006), 307–335, [hep-ex/0508060].

- [21] G. Aad et al., ATLAS, *Measurement of the angular coefficients in Z-boson events using electron and muon pairs from data taken at $\sqrt{s} = 8$ TeV with the ATLAS detector*, JHEP **08** (2016), 159, [[arXiv:1606.00689](#)] [[hep-ex](#)].
- [22] G. Aad et al., ATLAS, *Measurement of angular correlations in Drell-Yan lepton pairs to probe Z/gamma* boson transverse momentum at $\sqrt{s}=7$ TeV with the ATLAS detector*, Phys. Lett. B **720** (2013), 32–51, [[arXiv:1211.6899](#)] [[hep-ex](#)].
- [23] V. Khachatryan et al., CMS, *Angular coefficients of Z bosons produced in pp collisions at $\sqrt{s} = 8$ TeV and decaying to $\mu^+\mu^-$ as a function of transverse momentum and rapidity*, Phys. Lett. B **750** (2015), 154–175, [[arXiv:1504.03512](#)] [[hep-ex](#)].
- [24] R. Aaij et al., LHCb, *First Measurement of the $Z \rightarrow \mu^+\mu^-$ Angular Coefficients in the Forward Region of pp Collisions at $\sqrt{s} = 13$ GeV*, Phys. Rev. Lett. **129** (2022), no. 9, 091801, [[arXiv:2203.01602](#)] [[hep-ex](#)].
- [25] T. Aaltonen et al., CDF, *First Measurement of the Angular Coefficients of Drell-Yan e^+e^- pairs in the Z Mass Region from $p\bar{p}$ Collisions at $\sqrt{s} = 1.96$ TeV*, Phys. Rev. Lett. **106** (2011), 241801, [[arXiv:1103.5699](#)] [[hep-ex](#)].
- [26] T. Aaltonen et al., CDF, *Indirect Measurement of $\sin^2\theta_W (M_W)$ Using e^+e^- Pairs in the Z-Boson Region with $p\bar{p}$ Collisions at a Center-of-Momentum Energy of 1.96 TeV*, Phys. Rev. D **88** (2013), no. 7, 072002, [[arXiv:1307.0770](#)] [[hep-ex](#)], [Erratum: Phys.Rev.D 88, 079905 (2013)].
- [27] S. Schael et al., ALEPH, DELPHI, L3, OPAL, SLD, LEP Electroweak Working Group, SLD Electroweak Group, SLD Heavy Flavour Group, *Precision electroweak measurements on the Z resonance*, Phys. Rept. **427** (2006), 257–454, [[hep-ex/0509008](#)].
- [28] D. Acosta et al., CDF, *Measurement of the azimuthal angle distribution of leptons from W boson decays as a function of the W transverse momentum in $p\bar{p}$ collisions at $\sqrt{s} = 1.8$ TeV*, Phys. Rev. D **73** (2006), 052002, [[hep-ex/0504020](#)].
- [29] G. Aad et al., ATLAS, *Measurement of the polarisation of W bosons produced with large transverse momentum in pp collisions at $\sqrt{s} = 7$ TeV with the ATLAS experiment*, Eur. Phys. J. C **72** (2012), 2001, [[arXiv:1203.2165](#)] [[hep-ex](#)].
- [30] S. Chatrchyan et al., CMS, *Measurement of the Polarization of W Bosons with Large Transverse Momenta in $W+Jets$ Events at the LHC*, Phys. Rev. Lett. **107** (2011), 021802, [[arXiv:1104.3829](#)] [[hep-ex](#)].
- [31] D. Wackerth and W. Hollik, *Electroweak radiative corrections to resonant charged gauge boson production*, Phys. Rev. D **55** (1997), 6788–6818, [[hep-ph/9606398](#)].
- [32] U. Baur, S. Keller and W. K. Sakumoto, *QED radiative corrections to Z boson production and the forward backward asymmetry at hadron colliders*, Phys. Rev. D **57** (1998), 199–215, [[hep-ph/9707301](#)].
- [33] U. Baur, S. Keller and D. Wackerth, *Electroweak radiative corrections to W boson production in hadronic collisions*, Phys. Rev. D **59** (1999), 013002, [[hep-ph/9807417](#)].
- [34] U. Baur, O. Brein, W. Hollik, C. Schappacher and D. Wackerth, *Electroweak radiative corrections to neutral current Drell-Yan processes at hadron colliders*, Phys. Rev. D **65** (2002), 033007, [[hep-ph/0108274](#)].
- [35] U. Baur and D. Wackerth, *Electroweak radiative corrections to $p\bar{p} \rightarrow W^\pm \rightarrow \ell^\pm\nu$ beyond the pole approximation*, Phys. Rev. D **70** (2004), 073015, [[hep-ph/0405191](#)].
- [36] A. Andonov, A. Arbuzov, D. Bardin, S. Bondarenko, P. Christova, L. Kalinovskaya, G. Nanava and W. von Schlippe, *SANCScope - v.1.00*, Comput. Phys. Commun. **174** (2006), 481–517, [[hep-ph/0411186](#)], [Erratum: Comput.Phys.Commun. 177, 623–624 (2007)].
- [37] S. Dittmaier and M. Krämer, *Electroweak radiative corrections to W boson production at hadron colliders*, Phys. Rev. D **65** (2002), 073007, [[hep-ph/0109062](#)].

- [38] S. Dittmaier and M. Huber, *Radiative corrections to the neutral-current Drell-Yan process in the Standard Model and its minimal supersymmetric extension*, JHEP **01** (2010), 060, [[arXiv:0911.2329 \[hep-ph\]](#)].
- [39] Y. Li and F. Petriello, *Combining QCD and electroweak corrections to dilepton production in FEWZ*, Phys. Rev. D **86** (2012), 094034, [[arXiv:1208.5967 \[hep-ph\]](#)].
- [40] S. Alioli et al., *Precision studies of observables in $pp \rightarrow W \rightarrow l\nu_l$ and $pp \rightarrow \gamma, Z \rightarrow l^+l^-$ processes at the LHC*, Eur. Phys. J. **C77** (2017), no. 5, 280, [[arXiv:1606.02330 \[hep-ph\]](#)].
- [41] R. Bonciani, L. Buonocore, M. Grazzini, S. Kallweit, N. Rana, F. Tramontano and A. Vicini, *Mixed Strong-Electroweak Corrections to the Drell-Yan Process*, Phys. Rev. Lett. **128** (2022), no. 1, 012002, [[arXiv:2106.11953 \[hep-ph\]](#)].
- [42] L. Buonocore, M. Grazzini, S. Kallweit, C. Savoini and F. Tramontano, *Mixed QCD-EW corrections to $pp \rightarrow \ell\nu_\ell + X$ at the LHC*, Phys. Rev. D **103** (2021), 114012, [[arXiv:2102.12539 \[hep-ph\]](#)].
- [43] T. Armadillo, R. Bonciani, S. Devoto, N. Rana and A. Vicini, *Two-loop mixed QCD-EW corrections to neutral current Drell-Yan*, JHEP **05** (2022), 072, [[arXiv:2201.01754 \[hep-ph\]](#)].
- [44] M. Delto, M. Jaquier, K. Melnikov and R. Röntsch, *Mixed QCD \otimes QED corrections to on-shell Z boson production at the LHC*, JHEP **01** (2020), 043, [[arXiv:1909.08428 \[hep-ph\]](#)].
- [45] F. Buccioni, F. Caola, M. Delto, M. Jaquier, K. Melnikov and R. Röntsch, *Mixed QCD-electroweak corrections to on-shell Z production at the LHC*, Phys. Lett. B **811** (2020), 135969, [[arXiv:2005.10221 \[hep-ph\]](#)].
- [46] R. Bonciani, F. Buccioni, N. Rana and A. Vicini, *Next-to-Next-to-Leading Order Mixed QCD-Electroweak Corrections to on-Shell Z Production*, Phys. Rev. Lett. **125** (2020), no. 23, 232004, [[arXiv:2007.06518 \[hep-ph\]](#)].
- [47] R. Bonciani, F. Buccioni, N. Rana and A. Vicini, *On-shell Z boson production at hadron colliders through $\mathcal{O}(\alpha_s)$* , JHEP **02** (2022), 095, [[arXiv:2111.12694 \[hep-ph\]](#)].
- [48] A. Behring, F. Buccioni, F. Caola, M. Delto, M. Jaquier, K. Melnikov and R. Röntsch, *Mixed QCD-electroweak corrections to W-boson production in hadron collisions*, Phys. Rev. D **103** (2021), no. 1, 013008, [[arXiv:2009.10386 \[hep-ph\]](#)].
- [49] S. Dittmaier, A. Huss and C. Schwinn, *Mixed QCD-electroweak $\mathcal{O}(\alpha_s\alpha)$ corrections to Drell-Yan processes in the resonance region: pole approximation and non-factorizable corrections*, Nucl. Phys. B **885** (2014), 318–372, [[arXiv:1403.3216 \[hep-ph\]](#)].
- [50] S. Dittmaier, A. Huss and C. Schwinn, *Dominant mixed QCD-electroweak $\mathcal{O}(\alpha_s\alpha)$ corrections to Drell-Yan processes in the resonance region*, Nucl. Phys. B **904** (2016), 216–252, [[arXiv:1511.08016 \[hep-ph\]](#)].
- [51] M. H. Seymour, *Photon radiation in final state parton showering*, Z. Phys. C **56** (1992), 161–170, CAVENDISH-HEP-91-16.
- [52] D. R. Yennie, S. C. Frautschi and H. Suura, *The infrared divergence phenomena and high-energy processes*, Annals Phys. **13** (1961), 379–452.
- [53] J. Bellm et al., *Herwig 7.2 release note*, Eur. Phys. J. C **80** (2020), no. 5, 452, [[arXiv:1912.06509 \[hep-ph\]](#)].
- [54] J. Bellm et al., *Herwig 7.0/Herwig++ 3.0 release note*, Eur. Phys. J. C **76** (2016), no. 4, 196, [[arXiv:1512.01178 \[hep-ph\]](#)].
- [55] C. Bierlich et al., *A comprehensive guide to the physics and usage of PYTHIA 8.3*, [arXiv:2203.11601 \[hep-ph\]](#).
- [56] T. Sjöstrand, S. Ask, J. R. Christiansen, R. Corke, N. Desai, P. Ilten, S. Mrenna, S. Prestel, C. O. Rasmussen and P. Z. Skands, *An introduction to PYTHIA 8.2*, Comput. Phys. Commun. **191** (2015), 159–177, [[arXiv:1410.3012 \[hep-ph\]](#)].

- [57] S. Höche, S. Schumann and F. Siegert, *Hard photon production and matrix-element parton-shower merging*, Phys. Rev. D **81** (2010), 034026, [[arXiv:0912.3501](#) [hep-ph]].
- [58] T. Gleisberg, S. Höche, F. Krauss, M. Schönherr, S. Schumann, F. Siegert and J. Winter, *Event generation with SHERPA 1.1*, JHEP **02** (2009), 007, [[arXiv:0811.4622](#) [hep-ph]].
- [59] E. Bothmann et al., *Event Generation with SHERPA 2.2*, 2019.
- [60] K. Hamilton and P. Richardson, *Simulation of QED radiation in particle decays using the YFS formalism*, JHEP **07** (2006), 010, [[hep-ph/0603034](#)].
- [61] M. Schönherr and F. Krauss, *Soft Photon Radiation in Particle Decays in SHERPA*, JHEP **12** (2008), 018, [[arXiv:0810.5071](#) [hep-ph]].
- [62] F. Krauss, J. M. Lindert, R. Linten and M. Schönherr, *Accurate simulation of W, Z and Higgs boson decays in Sherpa*, Eur. Phys. J. C **79** (2019), no. 2, 143, [[arXiv:1809.10650](#) [hep-ph]].
- [63] F. Krauss, A. Price and M. Schönherr, *YFS Resummation for Future Lepton-Lepton Colliders in SHERPA*, SciPost Phys. **13** (2022), no. 2, 026, [[arXiv:2203.10948](#) [hep-ph]].
- [64] C. M. Carloni Calame, *An Improved parton shower algorithm in QED*, Phys. Lett. B **520** (2001), 16–24, [[hep-ph/0103117](#)].
- [65] C. Carloni Calame, G. Montagna, O. Nicrosini and M. Treccani, *Higher order QED corrections to W boson mass determination at hadron colliders*, Phys. Rev. D **69** (2004), 037301, [[hep-ph/0303102](#)].
- [66] C. M. Carloni Calame, G. Montagna, O. Nicrosini and M. Treccani, *Multiple photon corrections to the neutral-current Drell-Yan process*, JHEP **05** (2005), 019, [[hep-ph/0502218](#)].
- [67] C. Carloni Calame, G. Montagna, O. Nicrosini and A. Vicini, *Precision electroweak calculation of the charged current Drell-Yan process*, JHEP **12** (2006), 016, [[hep-ph/0609170](#)].
- [68] C. M. Carloni Calame, G. Montagna, O. Nicrosini and A. Vicini, *Precision electroweak calculation of the production of a high transverse-momentum lepton pair at hadron colliders*, JHEP **10** (2007), 109, [[arXiv:0710.1722](#) [hep-ph]].
- [69] C. M. Carloni Calame, M. Chiesa, H. Martinez, G. Montagna, O. Nicrosini, F. Piccinini and A. Vicini, *Precision Measurement of the W-Boson Mass: Theoretical Contributions and Uncertainties*, Phys. Rev. D **96** (2017), no. 9, 093005, [[arXiv:1612.02841](#) [hep-ph]].
- [70] C. Bernaciak and D. Wackerroth, *Combining NLO QCD and Electroweak Radiative Corrections to W boson Production at Hadron Colliders in the POWHEG Framework*, Phys. Rev. D **85** (2012), 093003, [[arXiv:1201.4804](#) [hep-ph]].
- [71] L. Barze, G. Montagna, P. Nason, O. Nicrosini and F. Piccinini, *Implementation of electroweak corrections in the POWHEG BOX: single W production*, JHEP **04** (2012), 037, [[arXiv:1202.0465](#) [hep-ph]].
- [72] A. Mück and L. Oymanns, *Resonance-improved parton-shower matching for the Drell-Yan process including electroweak corrections*, JHEP **05** (2017), 090, [[arXiv:1612.04292](#) [hep-ph]].
- [73] L. Barze, G. Montagna, P. Nason, O. Nicrosini, F. Piccinini and A. Vicini, *Neutral current Drell-Yan with combined QCD and electroweak corrections in the POWHEG BOX*, Eur. Phys. J. C **73** (2013), no. 6, 2474, [[arXiv:1302.4606](#) [hep-ph]].
- [74] W. Placzek and S. Jadach, *Multiphoton radiation in leptonic W boson decays*, Eur. Phys. J. C **29** (2003), 325–339, [[hep-ph/0302065](#)].
- [75] E. Barberio, B. van Eijk and Z. Was, *PHOTOS: A Universal Monte Carlo for QED radiative corrections in decays*, Comput. Phys. Commun. **66** (1991), 115–128, CERN-TH-5857-90.
- [76] E. Barberio and Z. Was, *PHOTOS: A Universal Monte Carlo for QED radiative corrections. Version 2.0*, Comput. Phys. Commun. **79** (1994), 291–308, CERN-TH-7033-93.

- [77] P. Golonka and Z. Was, *PHOTOS Monte Carlo: A Precision tool for QED corrections in Z and W decays*, Eur. Phys. J. C **45** (2006), 97–107, [[hep-ph/0506026](#)].
- [78] N. Davidson, T. Przedzinski and Z. Was, *PHOTOS interface in C++: Technical and Physics Documentation*, Comput. Phys. Commun. **199** (2016), 86–101, [[arXiv:1011.0937](#) [hep-ph]].
- [79] C. Gütschow and M. Schönherr, *Four lepton production and the accuracy of QED FSR*, Eur. Phys. J. C **81** (2021), no. 1, 48, [[arXiv:2007.15360](#) [hep-ph]].
- [80] A. V. Kotwal and B. Jayatilaka, *Comparison of HORACE and PHOTOS Algorithms for Multiphoton Emission in the Context of W Boson Mass Measurement*, Adv. High Energy Phys. **2016** (2016), 1615081, [[arXiv:1510.02458](#) [hep-ph]].
- [81] C. M. Carloni Calame, S. Jadach, G. Montagna, O. Nicrosini and W. Placzek, *Comparisons of the Monte Carlo programs HORACE and WINHAC for single W boson production at hadron colliders*, Acta Phys. Polon. B **35** (2004), 1643–1674, [[hep-ph/0402235](#)].
- [82] A. Arbuzov, R. Sadykov and Z. Was, *QED Bremsstrahlung in decays of electroweak bosons*, Eur. Phys. J. C **73** (2013), no. 11, 2625, [[arXiv:1212.6783](#) [hep-ph]].
- [83] S. Antropov, A. Arbuzov, R. Sadykov and Z. Was, *Extra lepton pair emission corrections to Drell-Yan processes in PHOTOS and SANC*, Acta Phys. Polon. B **48** (2017), 1469, [[arXiv:1706.05571](#) [hep-ph]].
- [84] S. Schumann and F. Krauss, *A Parton shower algorithm based on Catani-Seymour dipole factorisation*, JHEP **03** (2008), 038, [[arXiv:0709.1027](#) [hep-ph]].
- [85] M. H. Seymour, *Matrix element corrections to parton shower algorithms*, Comput. Phys. Commun. **90** (1995), 95–101, [[hep-ph/9410414](#)].
- [86] T. Sjostrand, S. Mrenna and P. Z. Skands, *PYTHIA 6.4 Physics and Manual*, JHEP **05** (2006), 026, [[hep-ph/0603175](#)].
- [87] S. Catani, S. Dittmaier, M. H. Seymour and Z. Trocsanyi, *The Dipole formalism for next-to-leading order QCD calculations with massive partons*, Nucl. Phys. **B627** (2002), 189–265, [[arXiv:hep-ph/0201036](#) [hep-ph]].
- [88] S. Höche, S. Kuttimalai, S. Schumann and F. Siegert, *Beyond Standard Model calculations with Sherpa*, Eur. Phys. J. C **75** (2015), no. 3, 135, [[arXiv:1412.6478](#) [hep-ph]].
- [89] M. Schönherr, *An automated subtraction of NLO EW infrared divergences*, Eur. Phys. J. **C78** (2018), no. 2, 119, [[arXiv:1712.07975](#) [hep-ph]].
- [90] S. Dittmaier, A. Kabelschacht and T. Kasprzik, *Polarized QED splittings of massive fermions and dipole subtraction for non-collinear-safe observables*, Nucl. Phys. **B800** (2008), 146–189, [[arXiv:0802.1405](#) [hep-ph]].
- [91] S. Kallweit, J. M. Lindert, S. Pozzorini and M. Schönherr, *NLO QCD+EW predictions for $2\ell 2\nu$ diboson signatures at the LHC*, JHEP **11** (2017), 120, [[arXiv:1705.00598](#) [hep-ph]].
- [92] D. Amati, A. Bassetto, M. Ciafaloni, G. Marchesini and G. Veneziano, *A Treatment of Hard Processes Sensitive to the Infrared Structure of QCD*, Nucl. Phys. B **173** (1980), 429–455, CERN-TH-2831.
- [93] S. J. Brodsky, G. P. Lepage and P. B. Mackenzie, *On the Elimination of Scale Ambiguities in Perturbative Quantum Chromodynamics*, Phys. Rev. D **28** (1983), 228, SLAC-PUB-3011, FERMILAB-PUB-83-040-T.
- [94] M. Cacciari, G. P. Salam and G. Soyez, *The Anti- $k(t)$ jet clustering algorithm*, JHEP **04** (2008), 063, [[arXiv:0802.1189](#) [hep-ph]].
- [95] A. Buckley et al., *Rivet user manual*, Comput. Phys. Commun. **184** (2013), 2803–2819, [[arXiv:1003.0694](#) [hep-ph]].
- [96] C. Bierlich et al., *Robust Independent Validation of Experiment and Theory: Rivet version 3*, SciPost Phys. **8** (2020), 026, [[arXiv:1912.05451](#) [hep-ph]].

- [97] L. Basso, S. Dittmaier, A. Huss and L. Oggero, *Techniques for the treatment of IR divergences in decay processes at NLO and application to the top-quark decay*, Eur. Phys. J. **C76** (2016), no. 2, 56, [[arXiv:1507.04676](#) [hep-ph]].
- [98] S. Dittmaier, *A general approach to photon radiation off fermions*, Nucl. Phys. **B565** (2000), 69–122, [[arXiv:hep-ph/9904440](#) [hep-ph]].